CZECH TECHNICAL UNIVERSITY IN PRAGUE
Faculty of Nuclear Sciences and Physical Engineering
Department of Physics

Research project

Central exclusive production in proton-proton collisions

Author: Bc. Tomáš Truhlář
Supervisor: Włodzimierz Guryn, Ph.D
Consultant: doc. Mgr. Jaroslav Bielčík, Ph.D.
Year: 2019

ČESKÉ VYSOKÉ UČENÍ TECHNICKÉ
V PRAZE
Fakulta jaderná a fyzikálně inženýrská

Katedra Fyziky
Obor: Experimentální jaderná a částicová fyzika

Centrální exkluzivní produkce v proton-protonových srážkách

VÝZKUMNÝ ÚKOL

Vypracoval:	Bc. Tomáš Truhlář
Vedoucí práce:	Włodzimierz Guryn, Ph.D
Konzultant:	doc. Mgr. Jaroslav Bielčík, Ph.D.
Rok:	2019

ČESKÉ VYSOKÉ UČENÍ TECHNICKÉ V PRAZE
FAKULTA JADERNÁ A FYZIKÁLNĚ INŽENÝRSKÁ
PRAHA 1 - STARÉ MĚSTO, BŘEHOVÁ 7 - PSČ 115 19

Katedra: fyziky **Akademický rok:** 2018/2019

VÝZKUMNÝ ÚKOL

Student: Tomáš Truhlář

Studijní program: Aplikace přírodních věd

Obor: Experimentální jaderná a částicová fyzika

Vedoucí úkolu: Włodzimierz Guryn, Ph.D, Brookhavenská národní laboratoř

Mgr. Jaroslav Bielčík, Ph.D - konzultant

Název úkolu (česky/anglicky): Centrální exkluzivní produkce v proton-protonových srážkách

Central exclusive production in proton-proton collision

Pokyny pro vypracování:

1. Fyzika pomeronu a centrální exkluzivní produkce
2. Experiment STAR na urychlovači RHIC
3. Aktuální výsledky ve fyzice dopředných protonů
4. Analýza centrální exkluzivní produkce v proton-protonových srážkách
5. Diskuze

Práce bude vypracována v anglickém jazyce.
Součástí zadání výzkumného úkolu je jeho uložení na webové stránky katedry fyziky.

Literatura:

[1] S. Donnachie: Pomeron Physics and QCD, Cambridge University Press, 2002
[2] V. Barone: High-Energy Particle Diffraction, Text and Monographs in Physics, Springer Verlag, 2002
[3] M. Albrow, et al.: Central Exclusive Production in Hadron–Hadron Collisions, International Journal of Modern Physics A Vol. 29, No. 28 (2014)
[4] P. Lebiedowicz, et al.: Central exclusive production of K+ K− pairs in proton-proton collisions, arXiv:1810.01171, 2018

Datum zadání: 22.10.2018

Datum odevzdání: 28.06.2019

....
vedoucí katedry

Prohlášení

Prohlašuji, že jsem svůj Výzkumný úkol vypracoval samostatně a použil jsem pouze podklady (literaturu, projekty, SW atd.) uvedenou v přiloženém seznamu.

Nemám závažný důvod proti užití tohoto školního díla ve smyslu § 60 Zákona č. 121/2000 Sb., o právu autorském, o právech souvisejících s právem autorským a o změně některých zákonů (autorský zákon).

V Praze dne ....

Bc. Tomáš Truhlář

Acknowledgments

I would like to thank my supervisor Włodzimierz Guryn, Ph.D for his guidance, his patience and valuable advice. I would also like to thank my consultant doc. Mgr. Jaroslav Bielčík, Ph.D. for his constructive comments. Furthermore, I would like to thank Ing. Jaroslav Adam, Ph.D. and Rafal Sikora, M.Sc. for their important help with the analysis.

Bc. Tomáš Truhlář

Název práce:
Centrální exkluzivní produkce v proton-protonových srážkách

Autor: Bc. Tomáš Truhlář

Studijní program: Aplikace přírodních věd
Obor: Experimentální jaderná a částicová fyzika
Druh práce: Výzkumný úkol

Vedoucí práce: Włodzimierz Guryn, Ph.D, Brookhavenská národní laboratoř
Konzultant: doc. Mgr. Jaroslav Bielčík, Ph.D., Katedra Fyziky, Fakulta jaderná a fyzikálně inženýrská, České vysoké učení technické v Praze

Abstrakt: Urychlovače nabitých částic poskytují jedinečnou možnost ke studiu difrakčních procesů, jako je centrální exkluzivní produkce v proton-protonových srážkách. Tyto procesy jsou považovány za potenciální zdroj vázaných stavů gluonů, glueballů. Experimentální potvrzení jejich existence by silně podpořilo platnost kvantové chromodynamiky. V této práci je představeno první měření těchto procesů v proton-protonových srážkách v $\sqrt{s} = 510$ GeV naměřených na experimentu STAR. Měření difrakčně rozptýlených protonů pomocí detektorů Roman Pot poskytlo plnou kontrolu nad kinematikou interakce a umožnilo ověření exkluzivity. První výsledek ve formě distribuce invariantní hmotnosti centrálně produkovaných $\pi^+\pi^-$ párů je prezentován v této práci.

Klíčová slova: Pomeron, Glueball, RHIC, STAR, Roman Pot

Title: **Central exclusive production in proton-proton collisions**

Author: Bc. Tomáš Truhlář

Abstract: High energy colliders provide a unique opportunity to study diffractive processes such as central exclusive production in proton-proton collisions. These processes are considered to be a potential source of the gluon bound states, glueballs. The experimental confirmation of their existence would be a strong support for the validity of the quantum chromodynamics theory. This work is dedicated to the first measurement of those processes in proton-proton collisions at $\sqrt{s} = 510$ GeV collected by the STAR experiment. The measurement of diffractively scattered protons using Roman Pots detectors allows full control over interaction kinematics and verification of the exclusivity. The first result in the form of distribution of invariant mass of centrally produced $\pi^+\pi^-$ pairs is presented in this work.

Key words: Pomeron, Glueball, RHIC, STAR, Roman Pots

Contents

List of Figures

List of Tables

Introduction

Everything around us is composed of elementary particles such as quarks, leptons and bosons. The standard model of particle physics describes the way how the elementary particles form the matter around us using three of the four fundamental forces: electromagnetic, weak, and strong interactions. The strong interaction is described by the quantum chromodynamics (QCD) theory using gluons as the exchange particles. Together gluons and quarks are forming bound states e.g. proton or neutron which are a necessary part of each atom.

High energy colliders such as the Relativistic Heavy Ion Collider (RHIC) at the Brookhaven National Laboratory and the Large Hadron Collider at CERN provide a unique opportunity to study diffractive processes such as central exclusive production (CEP) in proton-proton collisions. In CEP, the protons emerge intact and central state is produced with quantum numbers of vacuum. It is believed that the Double $\mathbb{P}$omeron Exchange is dominant CEP mechanism at high energies. This gluon-rich environment is considered to be a potential source of the gluon bound states (glueballs). The experimental confirmation of the existence of the glueball would be yet another strong support for the validity of the QCD theory. However, the existence of a glueball has not been unambiguously confirmed yet, despite its theoretical predictions.

The main goal of this work is to validate the picoDST production and data from proton-proton collisions at $\sqrt{s} = 510$ GeV collected by the STAR experiment in 2017. Since the data contain triggers from D$\mathbb{P}$E in CEP, they are promising for glueball search.

The first chapter of this work is a brief theoretical introduction to the hadronic diffraction physics, Regge framework and CEP. The second chapter provides the summary of recent results in central exclusive production, achieved by the experiments at CERN and by the STAR experiment. The third chapter describes the Relativistic Heavy Ion Collider accelerator complex and the STAR experiment with its sub-detectors: Time Projection Chamber, Time of Flight detector, Beam-Beam Counter and Roman Pots. Finally, the fourth and last chapter of this work is dedicated to the first measurement of CEP in proton-proton collisions at $\sqrt{s} = 510$ GeV measured by the STAR experiment. Specifically, distribution of invariant mass of centrally produced $\pi^+\pi^-$ pairs is presented.

Chapter 1

Central exclusive production

Before central exclusive production is described, it is necessary to define kinematic variables and introduce theoretical framework.

1.1 Kinematics

Mandelstam variables are commonly used for descriptions of two-body reactions such as scattering processes of two particles to two particles which can be seen in Fig. 1.1. There are three Mandelstam variables defined as:

- $s = (p_1 + p_2)^2 = (p_3 + p_4)^2$,
- $t = (p_1 - p_3)^2 = (p_2 - p_4)^2$,
- $u = (p_1 - p_4)^2 = (p_2 - p_3)^2$,

where p_1, p_2 are four-momenta of incoming particles and p_3, p_4 are four-momenta of outgoing particles. Furthermore, the letters s, t, u stand for the channels corresponding to Feynman diagrams [1]. In the reaction $1 + 2 \rightarrow 3 + 4$ the Mandelstam variable s is square of the total center of mass energy and variable t is squared four momentum transfer [2].

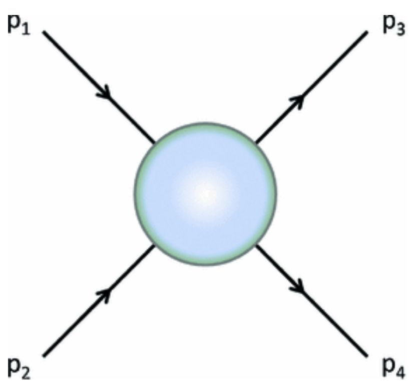

Fig. 1.1: The illustration of two-to-two particle scattering process. Taken from Ref. [3].

In high energy physics, rapidity y is often used to describe the longitudinal momentum of final-state particle, defined as

$$y = \frac{1}{2} \ln \frac{E + p_z c}{E - p_z c}, \tag{1.1}$$

where E is an energy of particle, p_z is longitudinal momentum of particle and c denotes the speed of light. The useful feature of rapidity is that it transforms additively under a Lorentz boost along z coordinate[1]. The rapidity y is often replaced by the pseudorapidity η which is defined as

$$\eta \equiv - \ln \tan \frac{\theta}{2}, \tag{1.2}$$

where the angle θ is a polar angle and specifies the direction of particle motion with respect to the z coordinate. The pseudorapidity and rapidity are approximately equal for massless particles and for particles with $|p_\mathrm{T}| \gg m$ [2] [2].

In the center-of-mass frame at high energy $\sqrt{s}$, the magnitude of the longitudinal momentum of each initial particle is almost equal to $\frac{1}{2}\sqrt{s}$. The longitudinal momentum p_z of a final-state particle can be than written as

$$p_z = \frac{1}{2} x_F \sqrt{s}, \tag{1.3}$$

where x_F is Feynman's variable defined as $x_F \equiv \frac{|p'_z|}{p_z}$ [2].

Another useful variable in CEP are $\xi = \Delta p / p$ the momentum fraction lost by a proton, hence it is equal to the momentum fraction carried off by the Pomeron and M_X the invariant mass of the centrally produced system. The M_X can be determined from the knowledge of incoming and outgoing protons momenta and from the four-momentum conservation [4].

1.2 Hadronic diffraction

High-energy particle diffractive processes are interactions between hadrons showing strong analogy with the same optical phenomenon. They were first introduced by Landau in the 1950's. They can be defined as a processes in which the outgoing system of particles at a given vertex has the same quantum numbers as the incoming one, hence no quantum numbers are exchanged between the colliding particles at high energies. Thus, they can be divided using the definition into 3 cases [2].

1. Elastic scattering, when incident particles emerge intact. See Fig. 1.2 (a).
2. Single diffraction dissociation (SDD), when one of the incident particles emerge intact and the other creates a number of final particles with the same quantum numbers as the initial particle. See Fig. 1.2 (b).

[1] z coordinate is parallel to the beam direction.
[2] p_T denotes particle's transverse momentum.

3. Double diffraction dissociation (DDD), when each incident particle creates a number of final particles with the same quantum numbers as the two initial particles. See Fig. 1.2 (c).

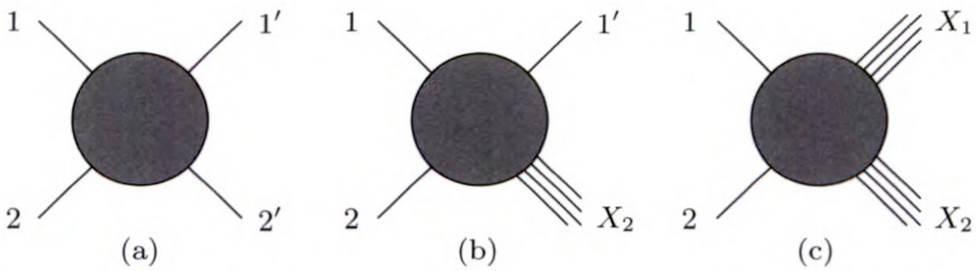

Fig. 1.2: The schematic view of diffractive processes: Elastic scattering (a), Single diffraction dissociation (b), Double diffraction dissociation (c). Taken from Ref. [2].

The definition above is quite unpractical, since it is difficult to fully reconstruct the final state and decide if the outgoing particles have the same quantum numbers as the incoming ones. Therefore, diffractive processes are redefined as non exponentially suppressed processes characterized by a large rapidity gap in the final state. This definition is equivalent to the first one and it is more practical since it is easier to measure rapidity gap than quantum numbers of particles. Although, the request of rapidity gap is practical, it is not sufficient condition. There are non-diffractive processes with large rapidity gap, however the number of these events is exponentially suppressed with increasing center-of-mass energy [2].

The diffractive processes can be divided based on the $|t|$-value in two classes [2]:

- The hard processes are processes with $|t| > 1$ GeV^2 and therefore they can be described by perturbative QCD.
- The soft processes are processes with $|t| < 1$ GeV^2 and with an energy scale of the order of the hadron size ~ 1 fm. Since, they have large length scale, the perturbative QCD is not suitable for description of these processes and Regge theory is used.

The exciting feature of diffractive processes is presence of soft and hard properties at the same time. The hard diffractive processes allow to study diffraction in a pertubative QCD and they open up the way to translate Regge theory into language of QCD [2].

1.3 Regge theory and $\mathbb{P}$omeron

The traditional theoretical framework for diffraction is Regge theory. It describes hadronic reactions at high energies in terms of the exchange of objects called reggeons or Regge trajectory $\alpha(t)$. Each family of bound states or resonances[3] corresponds

[3]Bound state which decade by the strong force are called resonances.

to a single Regge trajectory $\alpha(t)$. The Pomeron ($I\!P$) is reggeon with vacuum quantum numbers 0^{++} and intercept $\alpha_{I\!P}(0) = 1$. It is believed that diffractive processes at high energies are occurring via the exchange of $I\!P$. The $I\!P$ trajectory $\alpha_{I\!P}(t) = 1.08 + 0.25t/\mathrm{GeV}^2$ with a 2^{++} glueball candidate can be seen in Fig. 1.3 [5].

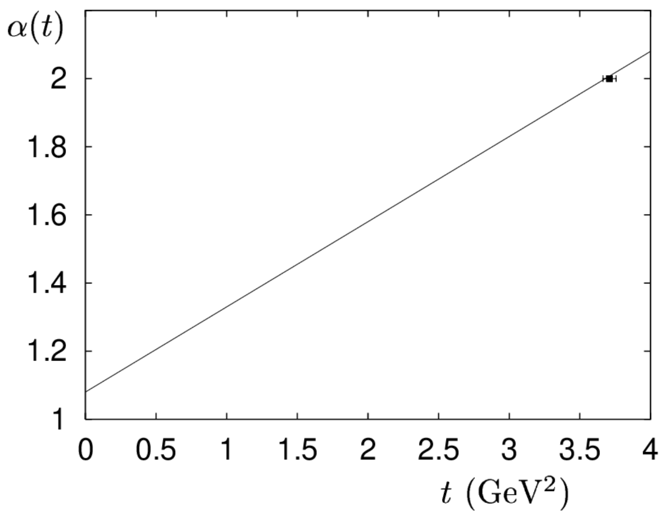

Fig. 1.3: The $I\!P$ trajectory $\alpha_{I\!P}(t) = 1.08+0.25t/\mathrm{GeV}^2$ with a 2^{++} glueball candidate. Taken from Ref. [5].

1.3.1 $I\!P$omeron

The $I\!P$omeron was named after Soviet theoretical physicist I. Ya. Pomeranchuk. Its existence was postulated by Chew, Frautschi and Gribov in 1961. However, the exact nature of the $I\!P$ still remains elusive. It is known that it is color singlet object with internal quantum numbers of the vacuum 0^{++}. The exchange of other reggeons with vacuum quantum numbers is suppressed at high energy. Thus in Regge theory the diffractive reactions are those dominated by $I\!P$ exchange [2, 5].

The $I\!P$ trajectory does not correspond to any known particle. However, in perturbative QCD in the leading order the $I\!P$ is represented by a pair of gluons since two gluons is the minimal number of gluons needed to reproduces the $I\!P$ quantum numbers. This representation was proposed by Low and Nussinow [2, 5].

1.3.2 Glueball

QCD predicts the existence of mesons which contain only gluons. These mesons (gluon bound states) are called glueballs. As a potential source of glueballs has been regarded the production of mesons in the central region of proton-proton scattering. Despite its theoretical predictions, the glueball has not yet been observed. The experimental confirmation of its existence would be yet another strong support for the validity of the QCD theory [4–6].

Lattice QCD calculations have predicted the lowest-lying scalar glueball state in the mass range of $1,500-1,700$ MeV/c^2 and tensor and pseudo-scalar glueballs in $2,000-2,500$ MeV/c^2. Experimentally measured glueball candidates for the scalar glueball states are the $f_0(1500)$ and the $f_1(1710)$ [4–6].

1.4 Central exclusive production

Central Exclusive particle Production (CEP) is process $A+B \to A+X+B$, where the colliding particles A and B emerge intact, and for which all particles are fully measured. A process is central when the outgoing particles are well separated from the produced state X by rapidity gap $\Delta y > 3$. The diagram of central exclusive production through double $\mathbb{P}$omeron exchange (D$\mathbb{P}$E) compare to the diagram of elastic scattering in proton-proton collisions with $\eta-\phi$ representations can be seen in Fig. 1.4 [6]. The first hadron collider measuring CEP was the CERN Intersecting Storage Rings (ISR) [7].

As Robson first suggested in 1977 [8], the D$\mathbb{P}$E is expected to be the dominant CEP mechanism at high center-of-mass energies. This processes do not involve valance quarks and the properties of the produced state X should be independent of the colliding hadrons. Furthermore, the produced state X must have $CP = ++$, total charge $Q = 0$ and even spin. D$\mathbb{P}$E was first observed at the ISR and since then it has been studied at numerous colliders such as the Sp$\bar{\text{p}}$S collider at CERN, the Tevatron at Fermilab, the Relativistic Heavy Ion Collider at Brookhaven National Laboratory and last but not least at the Large Hadron Collider at CERN [9].

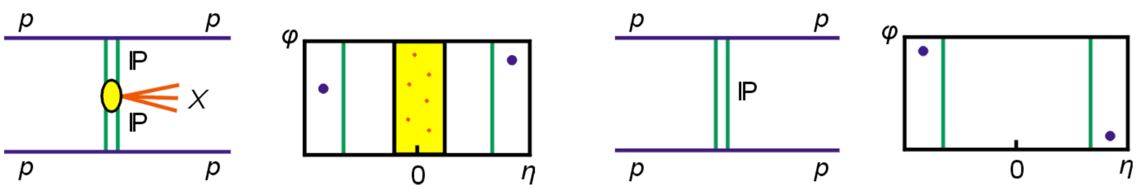

Fig. 1.4: Left: the diagram of central exclusive production through double Pomeron exchange with $\eta-\phi$ representation. Right: the diagram of elastic scattering with $\eta-\phi$ representation. Taken from Ref. [4].

Chapter 2

Results in central exclusive production

Before the CERN Intersecting Storage Rings (ISR), the world's first hadron collider, there were searches for DIPE in fixed target experiments. One of them was carried by the France-Soviet Union Collaboration at Serpukov [10]. They were only able to measure upper limits of the DIPE cross section. The ISR was the first to measure the DIPE in central exclusive production [11] since it had enough central mass energy for the DIPE signal to appear. At the ISR, there were many collaboration searching for DIPE: the ARCGM Collaboration, the CCHK Collaboration, the CHOV Collaboration, the CHM Collaboration and the AFS Collaboration. The ARCGM Collaboration was first which presented the experimental evidence of DIPE. The forward protons were tracked by all collaborations and only some collaborations measure their momenta. All collaborations, except the ARCGM, measured momenta of central particles, however only the AFS Collaboration identified them, otherwise pions were assumed. The DIPE measurements of the ISR collaborations are summarized in Tab. 2.1 [6].

Collaboration	$\sqrt{s}$ [GeV]	Central system	σ_{DIPE} [μb]
ARCGM	31	$\pi^+\pi^-$ [a]	28 ± 8
ARCGM	62	$\pi^+\pi^-$ [a]	20 ± 3
CCHK	31	$\pi^+\pi^-$ [a]	25 ± 10
CCHK	62	$\pi^+\pi^-$ [a]	12 ± 3
CHOV	23	$\pi^+\pi^-$ [a]	7 ± 1
CHOV	45	$\pi^+\pi^-$ [a]	6 ± 2
AFS	63	$\pi^+\pi^-$	34 ± 14 [b]
AFS	63	$\pi^+\pi^-$	1.9 ± 0.9 [c]
AFS	63	K^+K^-	1.4 ± 0.6
AFS	63	$p\bar{p}$	0.04 ± 0.2
AFS	63	$\pi^+\pi^-\pi^+\pi^-$	3 ± 2

Tab. 2.1: Summary of DIPE cross sections measured by the ISR collaborations. [a] The central system was not identified, just assumed. [b] For $M_{\pi\pi} < 1$ GeV/c^2. [b] For 1 GeV/$c^2 < M_{\pi\pi} < 2.3$ GeV/c^2. Taken from Ref. [6].

The AFS Collaboration also looked for glueballs in the reaction $p + p \to p + \pi^+\pi^- + p$ which is the most suitable reaction satisfying the quantum number filter for glueball search. The measured invariant mass spectra of $\pi^+\pi^-$ is shown in Fig. 2.1. The measured invariant mass spectra of $\pi^+\pi^-$ shows several interesting features. There is an rapid increase followed by a sharp drop at 1 GeV$/c^2$ and a bump between 1100 and 1500 MeV$/c^2$. There is no sign of ρ^0 decaying to $\pi^+\pi^-$ at 770 MeV$/c^2$, which is forbidden in DIPE. The interpretation of these features is not clear. It is believed that the rapid increase with sharp drop at 1 GeV$/c^2$ could be due to $f_0(600)$ and $f_0(980)$ resonances, which are the lightest scalar glueball candidates. The bump between 1100 and 1500 MeV$/c^2$ is considered to be $f_2(1270)$ resonance. According to Minkowski and Ochs, there is a single very broad state extending from 400 MeV$/c^2$ to about 1700 MeV$/c^2$. They call it red dragon and considering to be the lightest scalar glueball. Besides $\pi^+\pi^-$ CEP processes, the AFS Collaboration also measured CEP processes with K^+K^-, $p\bar{p}$ and $\pi^+\pi^-\pi^+\pi^-$ [6].

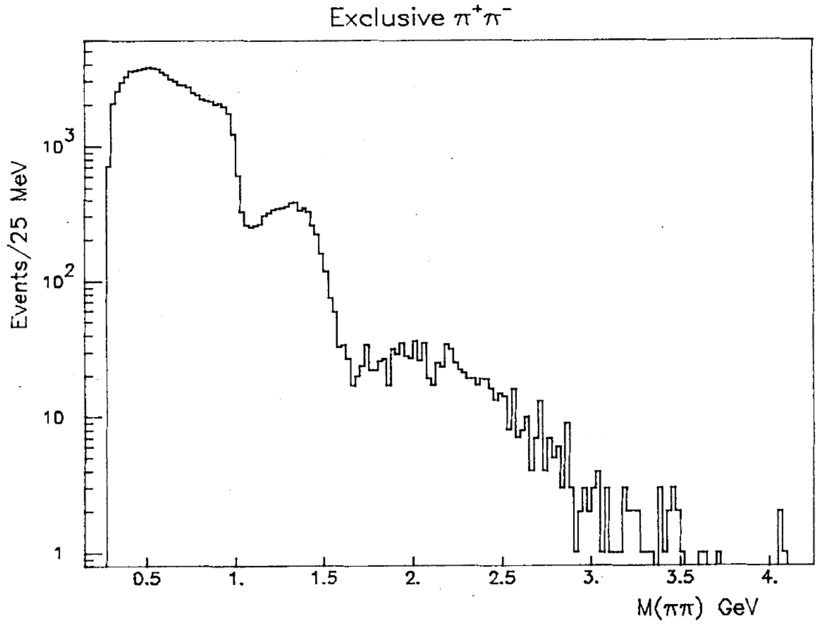

Fig. 2.1: The $\pi^+\pi^-$ invariant mass distribution measured by the AFS Collaboration at the Intersecting Storage Rings. Taken from Ref. [12].

At present, the CEP processes are studied at the STAR experiment and at CERN experiments: COMPASS, LHCb, ALICE, CMS and ATLAS. Nevertheless experiment such as LHCb, ALICE and CMS do not measure the outgoing protons and therefore they are not able to measure the exclusivity of the process. One of the newest measurements of those experiment was done by the CMS collaboration. They investigated CEP of $\pi^+\pi^-$ pairs in proton-proton collisions at the LHC at the $\sqrt{s} = 5.02$ and 13 TeV. They measured differential cross sections as a function of invariant mass of $\pi^+\pi^-$ which can be seen with four resonant peaks in Fig. 2.2. The measurement at 13 TeV is the first measurement of the CEP at that energy. The spectra shows similar features as in the spectra measured by the AFS Collaboration, especially the peak at 800 MeV$/c^2$ followed by the sharp drop 1000 MeV$/c^2$ and the peak at $1200-1300$ MeV$/c^2$. The first peak is attributed to $\rho^0(770)$ resonance. Since the isospin of ρ^0 is equal to one and the isospin of $\mathbb{P}$omeron is zero, the production of ρ^0 mesons in D$\mathbb{P}$E processes is forbidden by isospin and the ρ^0 mesons are produced in vector meson photoproduction (process, when $\mathbb{P}$omeron interacts with photon). The sharp drop is assigned to the interference of $f_0(980)$ with the continuum contribution and the second peak corresponds to the $f_2(1270)$ resonance. The measured differential cross sections is compared to the Dime Monte Carlo, a phenomenological model based on Regge theory describing the direct, nonresonant production of pion pairs via D$\mathbb{P}$E. Except the $\pi^+\pi^-$ spectra, the CMS also measured total exclusive $\pi^+\pi^-$ production cross sections $19.6 \pm 0.4(\text{stat.}) \pm 3.3(\text{syst.}) \pm 0.01(\text{lumi.})$ μb for 5.02 TeV and $19.0 \pm 0.6(\text{stat.}) \pm 3.2(\text{syst.}) \pm 0.01(\text{lumi.})$ μb for 13 TeV [13].

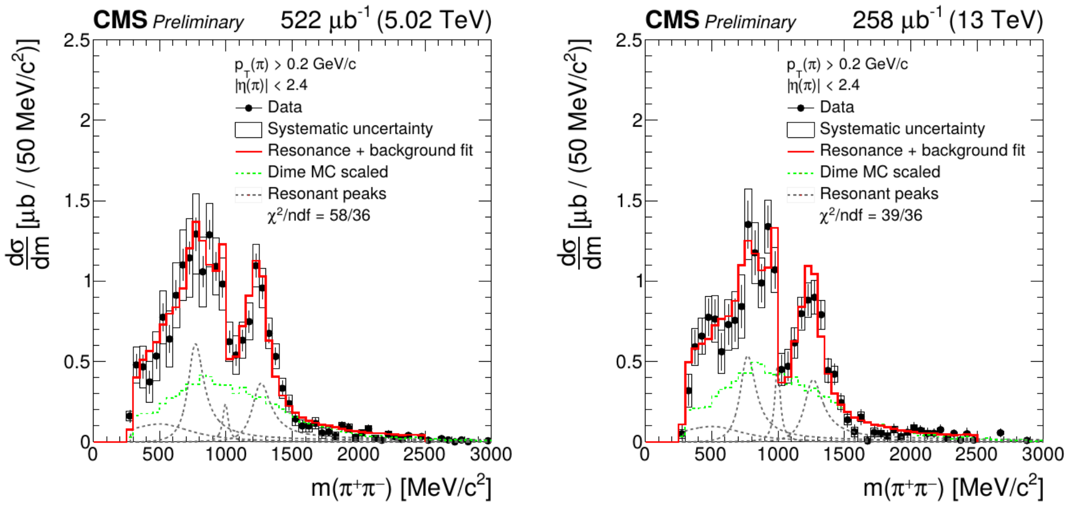

Fig. 2.2: The measured differential cross sections as a function of invariant mass of $\pi^+\pi^-$ for the 5.02 (left) and 13 TeV data sets. Taken from Ref. [13].

One of the most recent measurement of CEP with $\pi^+\pi^-$, K^+K^- pairs was done by the STAR experiment at the RHIC [14] in proton-proton collisions at $\sqrt{s} = 200$ GeV. Unlike the CMS Collaboration, the STAR experiment disposes with the Roman Pot detectors allowing efficient measurement of diffractively scattered protons, which enables full control over interaction kinematics and verification of the exclusivity of the reaction by measuring the total transverse momenta of all final state particles. The invariant mass spectra of exclusively produced $\pi^+\pi^-$ and K^+K^- with small squared momentum transfers $0.03 < |t_1|, |t_2| < 0.2$ GeV^2 were measured and they can be seen in Fig. 2.3. In general, we can see same features as in the spectra measured by the AFS Collaboration, however with much higher resolution. The $\pi^+\pi^-$ spectra was compared to models of non-resonant CEP that can qualitatively describe data only up to 0.7 GeV$/c^2$, which indicates significant role of resonance production. In the K^+K^- spectra, there is a noticeable peak at about 1.5 GeV$/c^2$ which can be interpreted as the $f_0(1500)$ state. There is also a bump at about 1.3 GeV$/c^2$ which can be the $f_2(1270)$ state, nevertheless the region is well describe by the non-resonance model [14].

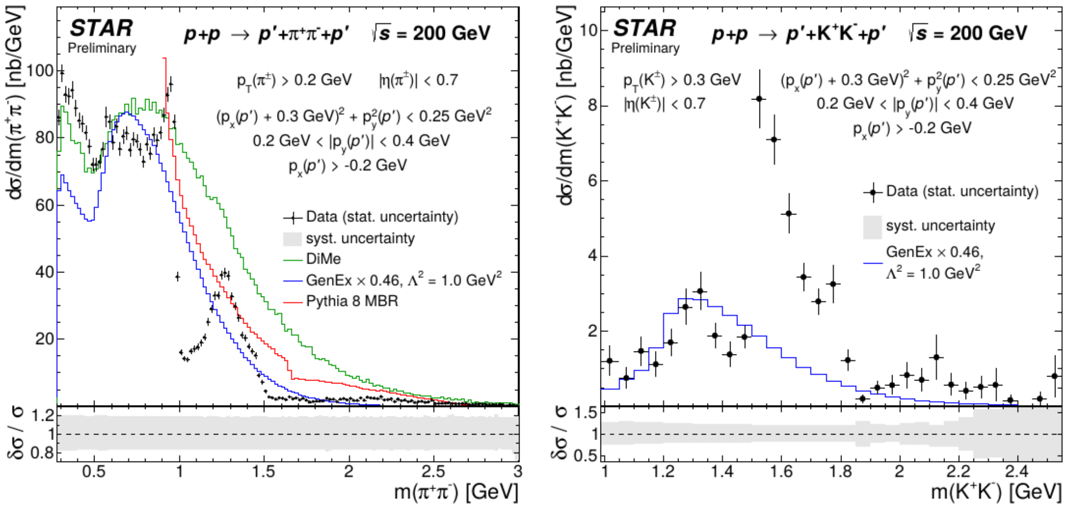

Fig. 2.3: Preliminary results on differential fiducial cross section as a function of invariant mass of $\pi^+\pi^-$ (left) and K^+K^- (right) compared to some models. Taken from Ref. [14].

Chapter 3

The STAR experiment at RHIC

3.1 Relativistic Heavy Ion Collider

In 1999, the Relativistic Heavy Ion Collider (RHIC) was built at Brookhaven National Laboratory in one of the biggest scientific facilities in the U.S. RHIC is was the first machine in the world capable of colliding heavy ions that allowed the studies of the Quark-Gluon Plasma. Furthermore, it is the only major accelerator capable of colliding polarized protons which allows measurements aimed at studying the spin structure of the proton [15, 16].

RHIC is consist of two rings with circumference of $3,834$ m where particles are accelerated in opposite directions, clockwise (blue) or counterclockwise (yellow). The rings intersect in 6 points called interaction points, where experiments are located. In 2000, there were 4 experiments: STAR, PHENIX, PHOBOS and BRAHMS. In 2002, the pp2pp experiment was added. The pp2pp was designed to study proton-proton elastic scattering from $\sqrt{s} = 60$ GeV to $\sqrt{s} = 510$ GeV via Roman Pot detectors. In 2009, it was incorporated into the STAR experiment, which is only one active experiment at present. Nevertheless, a new experiment sPHENIX is being prepared with planned launch in 2022 [15–17].

Before particles can be accelerated at RHIC they have to be pre-accelerated in pre-accelerator complex. The entire accelerator complex can be seen in Fig. 3.1. The protons are supplied by the Brookhaven Linear Accelerator (Linac). They continue to the Booster Synchrotron where they are accelerated to 2 GeV. Then, they are send to the Alternating Gradient Synchrotron (AGS) where they are accelerated further to 23 GeV. Finally, they are injected into RHIC where they are accelerated up to 255 GeV.

The ions start at the Laser Ion Source (LION) where they are transfered to the Electron Beam Ion Source (EBIS). Then, the ions are accelerated to 95 MeV/nucleon in the Booster Synchrotron. In the AGS they are further accelerated to 9 GeV/nucleon. Finally, they are injected into RHIC where they are accelerated up to 100 GeV/nucleon [15, 17, 18].

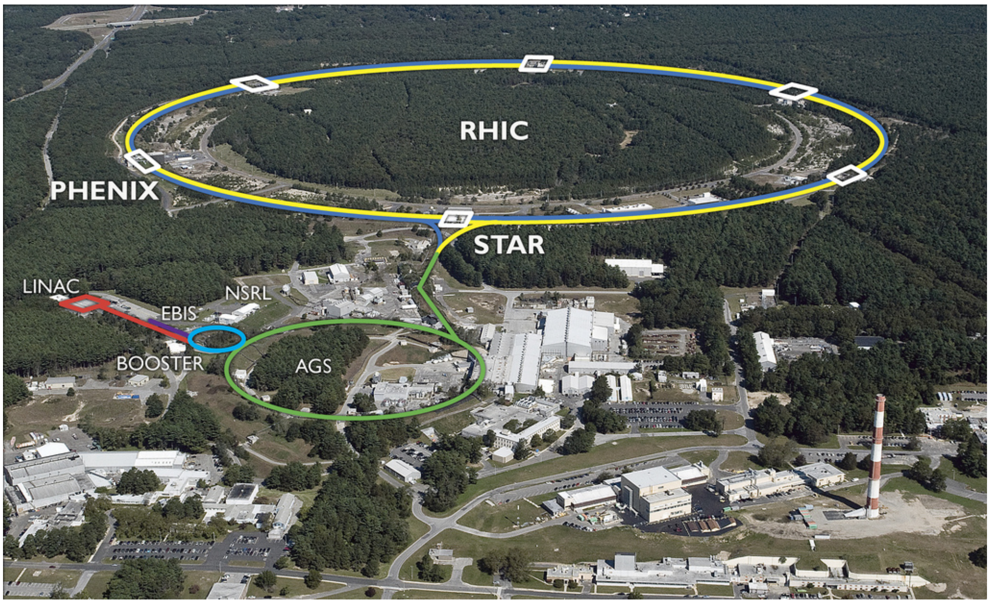

Fig. 3.1: The BNL accelerator complex consisting of multiple pre-accelerators and the main accelerator RHIC. Taken from Ref. [16].

3.2 Solenoidal Tracker at RHIC

The Solenoidal Tracker at RHIC (STAR) is large-acceptance multi-purpose particle detector designed to study the strongly interacting matter at high temperature and high energy density. It is massive detector weighting 1, 200 tuns consisting of many sub-detectors, such as the Time Projection Chamber (TPC), the Time of Flight detector (TOF), the Beam-Beam Counter (BBC), the Vertex Position Detector (VPD), the Barrel Electromagnetic Calorimeter (BEMC). Another important part of the experiment is a large solenoidal magnet covering full azimuthal angle and $|\eta| < 1$ in longitudinal direction and generating 0.5 T solenodial magnetic field parallel to the beam axis. The STAR experiment with its main sub-detectors is shown in Fig. 3.2 [17, 19].

The STAR experiment is very suitable for measuring CEP processes, because of its unique capabilities such as:

- high-resolution tracking of centrally produced charged particles in TPC,
- precise particle identification through the measurement of dE/dx and Time-of-Flight,
- forward rapidity $2.1 < |\eta| < 5.0$ covered by BBC detectors to ensure rapidity gap,
- Silicon Strip Detectors in Roman Pots for measurement of forward protons.

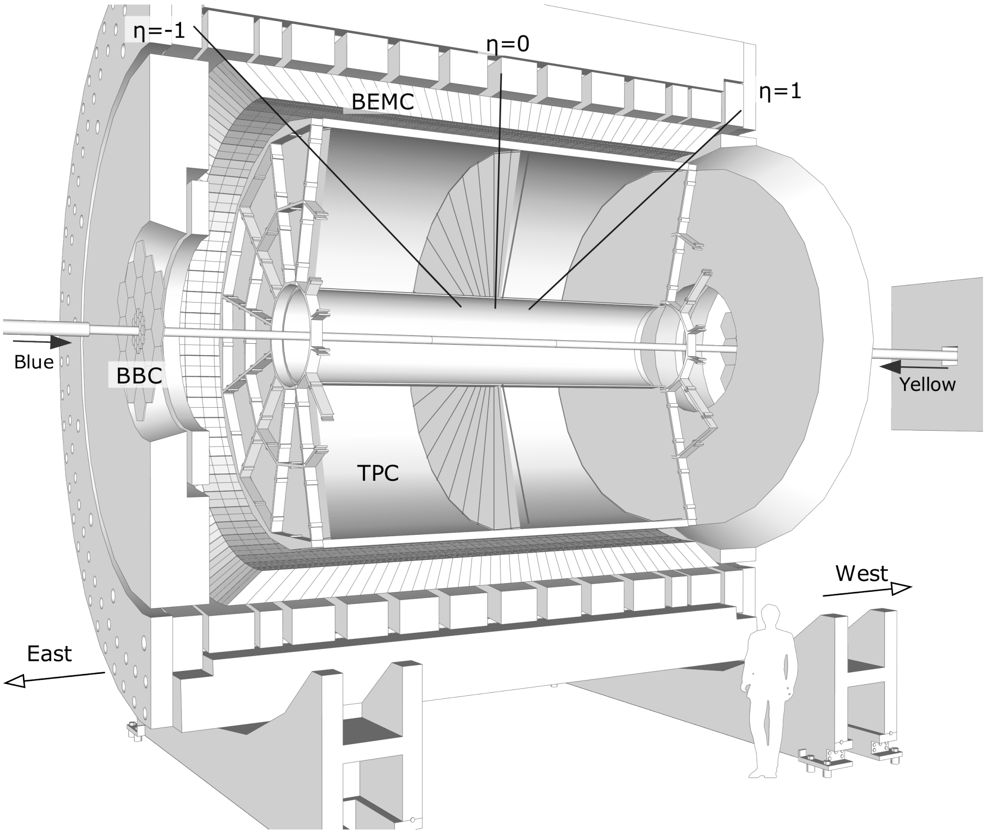

Fig. 3.2: The STAR experiment schematic view. Main sub-detectors, including TPC, TOF, BBC, VPD, BEMC are highlighted. Taken from Ref. [20].

3.2.1 Time Projection Chamber

The TPC is the heart of the STAR experiment. Its main purpose is precise particle identification and particle tracking. The schematic view of the TPC can be seen in Fig. 3.3. It is a large gas-filled cylindrical detector with inner diameter 1.0 m, outer diameter 4.0 m and 4.2 m long. It covers full azimuthal angle and pseudorapidity $|\eta| < 1.0$. The fill gas is P10 gas consisting of 90% argon and 10% methane. The P10 gas is kept at 2 mbar above the atmospheric pressure [21].

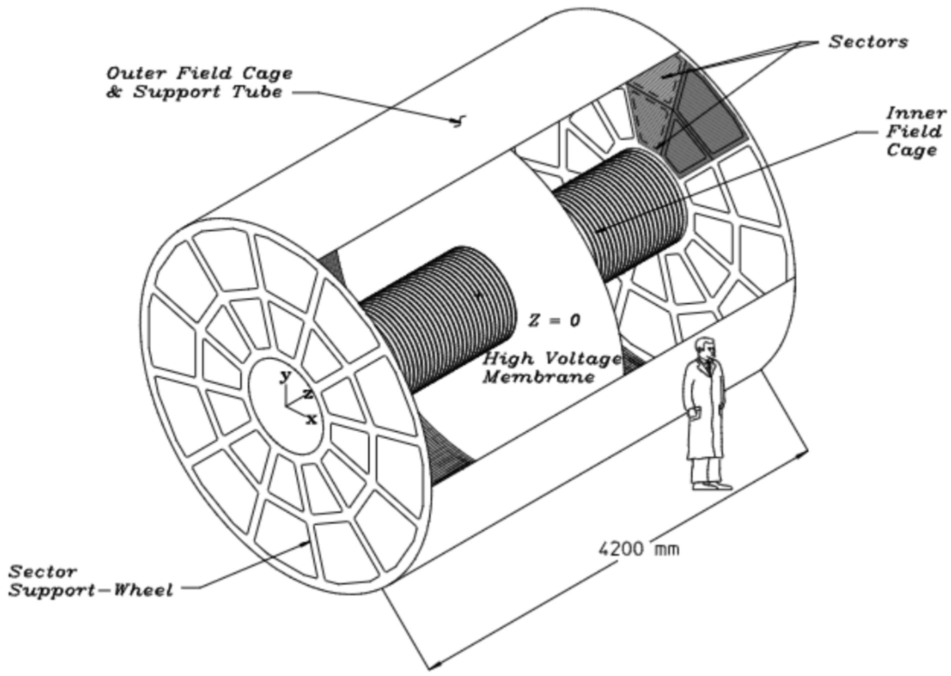

Fig. 3.3: The schematic view of the TPC. A person is shown for comparison. Taken from Ref. [21].

TPC is divided into two parts by high voltage conductive membrane, which is typically set to value of -28 kV. The membrane creates uniform electric field $E = 135$ V/cm. At both ends of the TPC, there are 48 Multi-Wire-Proportional-Chamber (MWPC) read-out sectors. A charged particle passing through the TPC creates electron-ion pairs and loose its energy. Then, the ions are moved towards the membrane and the electrons towards the MWPC sectors. Inside the MWPC sectors, the electrons are amplified by a factor of $1,000 - 3,000$. The detectable signal is collected and their drift time is measured. The typical electrons drift velocity is about 5.45 cm/μs and the drift time is approximately 40 μs [17, 21].

The STAR magnet provides magnetic field which curves the tracks of charged particles. Since the radius of track's curvature is proportional to the momentum of the particle, particle momentum can be measured over a range of 100 MeV/c to 30 GeV/c with the resolution about 2%.

Another important measurement obtained from TPC is ionization energy loss (dE/dx), which is used for particle identification (PID). The variable used in practice is:

$$n_\sigma = \frac{\ln \frac{\mathsf{d}E/\mathsf{d}x}{\langle \mathsf{d}E/\mathsf{d}x \rangle}}{R_{\mathsf{d}E/\mathsf{d}x}}, \tag{3.1}$$

where $\mathsf{d}E/\mathsf{d}x$ is an energy loss per unit length measured by the TPC, $\langle \mathsf{d}E/\mathsf{d}x \rangle$ is a mean energy loss per unit length for different particle species calculated using the Bichsel functions [22] and $R_{\mathsf{d}E/\mathsf{d}x}$ is the TPC resolution. The typical $\mathsf{d}E/\mathsf{d}x$ resolution of TPC of the STAR is 7%. The value of n_σ corresponds to the number of standard deviations between the measured and the theoretical energy loss for a given particle. In general, the TPC is able to identify particle with momenta from 100 MeV/c to − 1 GeV/c. An example of measurement and calculated energy loss of charged particles as a function of their momentum is shown in Fig. 3.4 [18,23,24].

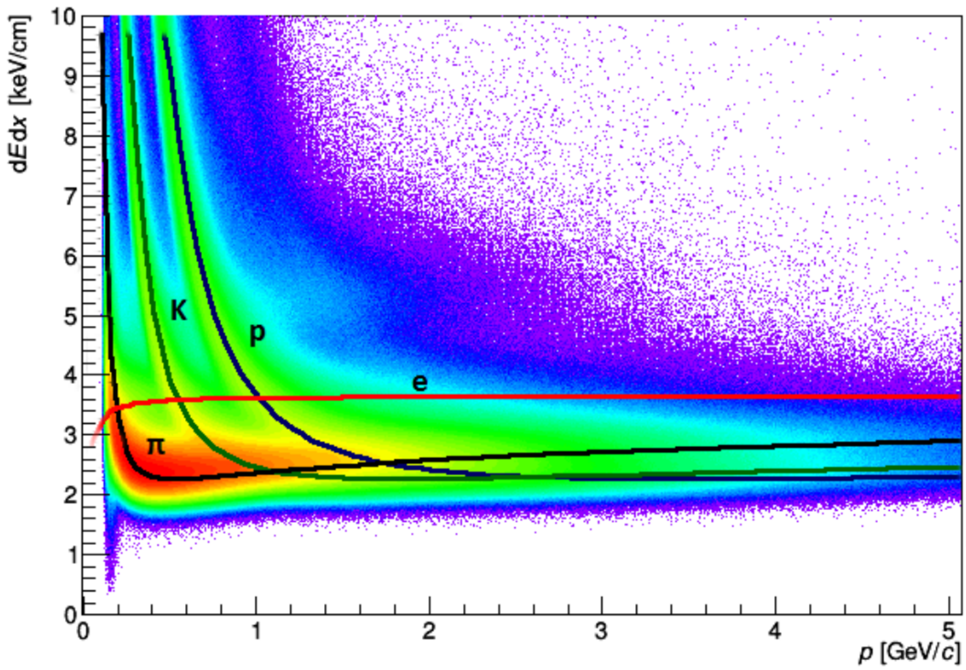

Fig. 3.4: The energy loss of charged particles as a function of their momentum. Expected values for electrons e, pions π, kaons K and protons p obtained from Bichsel functions [22] are shown as colored curves. Taken from Ref. [23].

3.2.2 Time of Flight detector

The main purpose of the TOF is to extend the PID capabilities of the TPC for particles with higher p_T. Furthermore, the TOF system is used in the trigger of the STAR experiment to select charged particle multiplicity in the central rapidity for various physics processes. For the CEP events it helps triggering on low multiplicity events in the TPC [25].

The TOF is a cylindrical shell around the TPC consisting of 120 trays and covering full azimuthal angle and the psuedorapidity $|\eta| < 1.0$. One tray is consisted of 32 Multi-gap Resistive Plate Chamber (MRPC) modules, which can be seen in

Fig. 3.5. The MRPC measures time, when particle passes through, with a resolution about 100 ps [26].

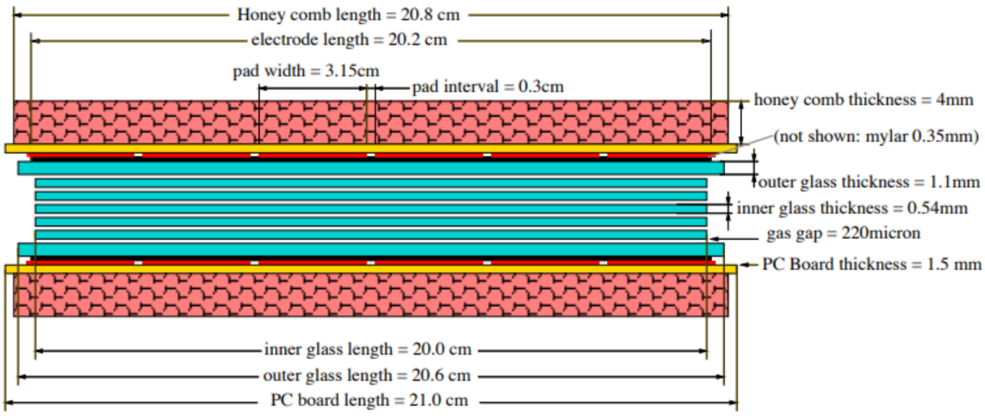

Fig. 3.5: A STAR Time Of Flight detector model with the dimensions shown. Taken from Ref. [25].

3.2.3 Beam-Beam Counter

The BBC is designed to detected particles with high pseudorapidity produced in $p+p$ collisions. The BBC is primarily used to monitor beam conditions and in the $p+p$ collisions used as the main trigger. The BBC detector at the STAR experiment is divided into two identical detectors located on the east and west sides of the interaction point at the distance about 374 cm. A schematic view of the BBC is shown in Fig. 3.6. Each detector consists of two inner annuli of 18 smaller scintillators and of two outer annuli of 18 larger scintillators. In the following chapter BBC stands for detectors consist of smaller scintillators and BBC Large denotes the detector consist of larger scintillators. Together it covers a pseudorapidity range of $2.1 < |\eta| < 5.0$ [18, 27].

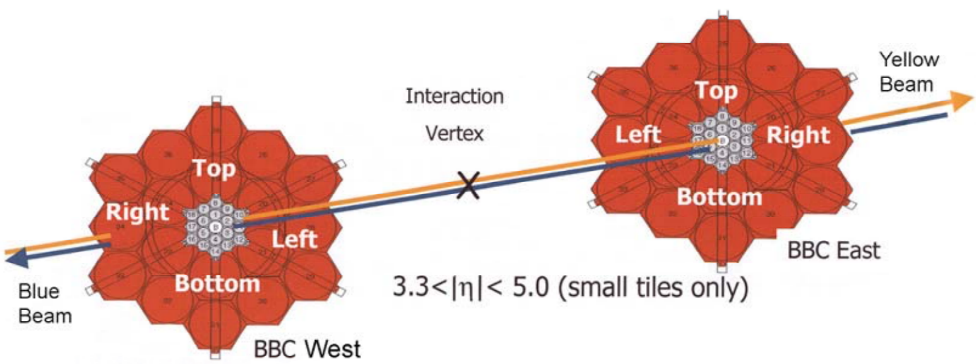

Fig. 3.6: The STAR BBC detector schematic view. The BBC is divided into two identical detectors on the east and west sides of the interaction point. Taken from Ref. [27].

3.3 Roman Pots

The Roman Pots (RPs) at the STAR experiment is system of forward detectors. They are used to detect and measure forward protons from elastic or inelastic scattering. The current layout of the RP system, called Phanse II*, is shown in Fig. 3.7. On each site of the interaction point, there are two RP stations at a distance of 15.8 m and 17.6 m. Each station consists of two RP vessels containing Silicon Strip Detector (SSD) package and a scintillation counter for trigger. The RP vessel and SSD package is shown in Fig. 3.8. The RP detectors are located between DX and D0 dipole magnets and they enable the reconstruction of the particle momentum by measuring the track angle and its position. Since the constant and uniform magnetic field of the DX magnet works as a spectrometer [28, 29].

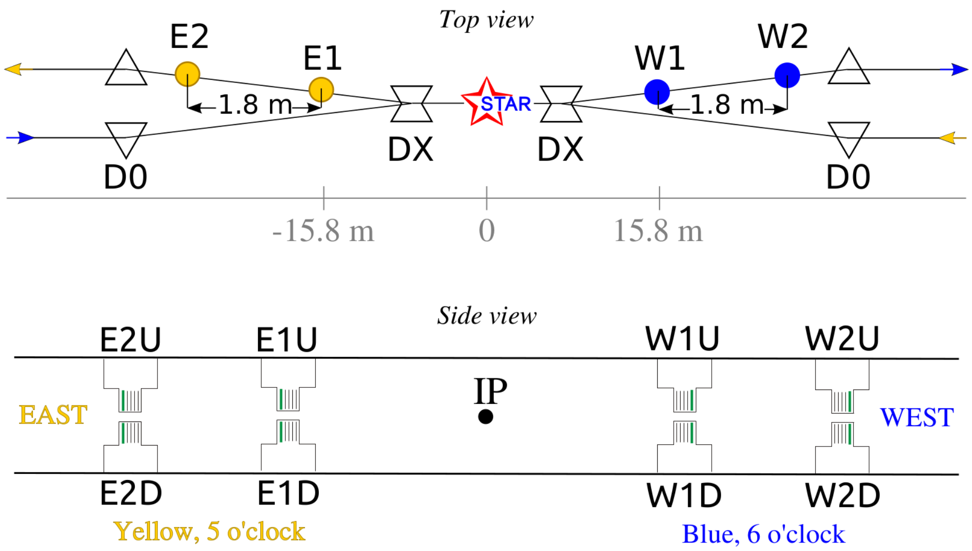

Fig. 3.7: The Roman Pot Phase II* layout. Top view with highlighted Roman Pot stations E1, E2, W1, W1 and dipole magnets DX, D0. Side view with depicted Roman Pots. Taken from Ref. [4].

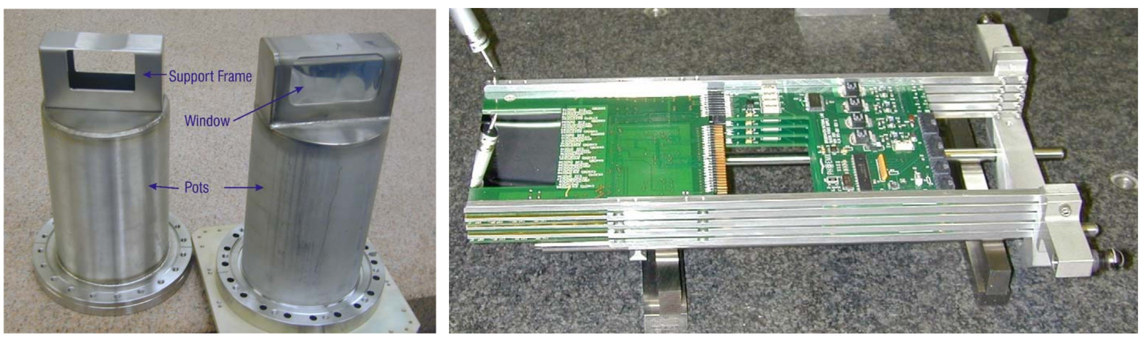

Fig. 3.8: The Roman pot vessels and the SSD package. Left: a photo of the two Roman Pots vessels. Main parts are indicated. Right: a photo of the Silicon Strip Detector package. Taken from Ref. [30].

The RP technology was first used at CERN's Intersecting Storage Rings in the early 1970s. Since, it has been successfully used in other colliders like the SPS, TEVATRON, RHIC, DESY and the LHC. Its main advantage is capability to measure scattered particles close to the beam in a distance of few millimeters from the beam with precision about 20 μm [29, 30].

At the STAR experiment, the detector is mounted inside RP steel vessel, which separates vacuum of the beampipe from the RP interior, which is mostly at atmospheric pressure. The RP vessel has pot, window and support frame, see Fig. 3.8. The window is made of 300 μm thick steel, which preventing damage from the beam vacuum or from the proton beam. A profile is designed to enable the closest approach of the pot to the beam [30, 31].

The detector package is a set of four silicon planes with the trigger scintillation counter. The set is called SSD package and it can be seen in Fig. 3.8. The silicon plane contains 6 SVXIIE readout chips with vertically oriented strips or 4 SVXIIE readout chips with horizontally oriented strips. The vertical plane is shown in Fig. 3.9. In the SSD package, the first and the third plane are horizontal ones and the second and the fourth plane are vertical ones. This ordering enables measuring of both coordinates of particle in the plane perpendicular to the beam direction. The strips cover active area of roughly 79 mm $\times$ 49 mm. Each SVXIIE readout chip reads 126 strips, which have $\sim$ 100 μm pitch allowing resolution of 30 μm. A scintillator covers whole active area of the detector and it is installed at the back of SSD package. It is used as the trigger and it also provides the timing information [28, 30].

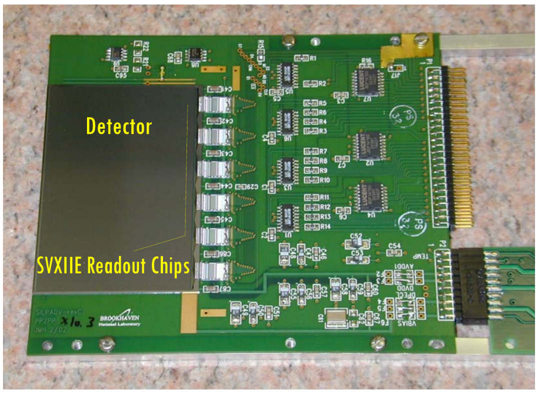

Fig. 3.9: A photo of the plane. Detector and SVXIIE readout chips are highlighted. Taken from Ref. [30].

Each RP has own name denoting precisely its position. The first letter indicate the site of the STAR detector where RP is mounted, E for "east", the "yellow" RHIC ring and W for "west", the "blue" RHIC ring. The second letter describes detector orientation, U means "up", RP is located above the beamline and D stands for "down", the RP is located below the beamline. Finally, there is a number 1 or 2 which denotes if it is the first one located in a distance of 15.8 m from interaction point or the second one located in a distance of 17.6 m from interaction point. For example the first RP located at the east site above the beamline is called E1U and it can be seen in Fig. 3.7.

Chapter 4

Analysis of central exclusive production in proton-proton collisions

In 2017, proton-proton collisions at $\sqrt{s} = 510$ GeV were collected by the STAR experiment. Since this data set contains triggers from DIPE in CEP, they are promising for glueball search. The goal of this analysis is to validate this data set. For this reason, data from run 17 RHICf period were used and a subset of 5% of data from the main data taking period. The rest of data is being produced so far. The RHICf data set contains data collected between June 25 and June 27. This data set is subset of whole data collected during year 2017 and it was priorly produced for testing reasons.

The data were stored in MuDst files which are produced from the raw data collected during the process of data taking. MuDst files contains all information about trajectories of centrally produced particles, outgoing protons. The MuDst files for all run 17 are bigger than 622 TB which make them very unpractical. For this reason we produced picoDST files containing only the most important information about the events and individual tracks reducing the size by factor of 100. I implemented all parts related to Roman Pots. Furthermore, I validated the new picoDST production by comparing with another version of picoDST files which was made by our colleagues from the AGH University of Science and Technology, Cracow, Poland.

In total, I analyzed $197,314,700$ events stored in muDst files from RHICf period and the first part of run 17 which was already produced. The part is containing about 5 % of all data from run 17. These first results of CEP at $\sqrt{s} = 510$ GeV are described in this chapter. The analysis was done using the ROOT framework and it was calculated on the STAR farm. The results marked as "this thesis" have not yet been approved by the STAR collaboration for public presentation.

4.1 Event selection

The goal was looking for the DIPE in CEP in $p+p \to p+\pi^+\pi^-+p$ collisions. The CEP is characterized by rapidity gap separating the outgoing protons from the central produced state. We required at least one of central productions triggers. There are 3 central productions triggers and they are described in Tab. 4.1. Generally, there is a requirement of only elastic or inelastic combination of outgoing protons in Roman Pots which they are shown in Fig. 4.1. Then, there is a requirement of hits in TOF ensuring centrally produced state. Finally, there is a requirement of no hits in ZDC, BBC or BBC Large ensuring rapidity gap between outgoing protons and centrally produced state.

Condition	CPT2		CPT2noBBCL		CPTnoBBCL	
Elastic combination in RP	$-$	$+$	$-$	$+$	$-$	$+$
Inelastic combination in RP	$+$	$-$	$+$	$-$	$+$	$-$
Number of TOF hits > 0	$+$	$+$	$+$	$+$	$\circ$	$\circ$
Number of TOF hits > 10	$-$	$-$	$-$	$-$	$\circ$	$\circ$
Number of TOF hits > 1	$\circ$	$\circ$	$\circ$	$\circ$	$+$	$+$
Hit in BBC east	$-$	$-$	$-$	$-$	$-$	$-$
Hit in BBC west	$-$	$-$	$-$	$-$	$-$	$-$
Hit in ZDC east	$-$	$-$	$-$	$-$	$-$	$-$
Hit in ZDC west	$-$	$-$	$-$	$-$	$-$	$-$
Hit in BBC Large east	$\circ$	$\circ$	$-$	$-$	$-$	$-$
Hit in BBC Large west	$\circ$	$\circ$	$-$	$-$	$-$	$-$

Tab. 4.1: Descriptions of central productions triggers. The $+$ means requirement while $-$ stands for veto and the $\circ$ denotes no condition.

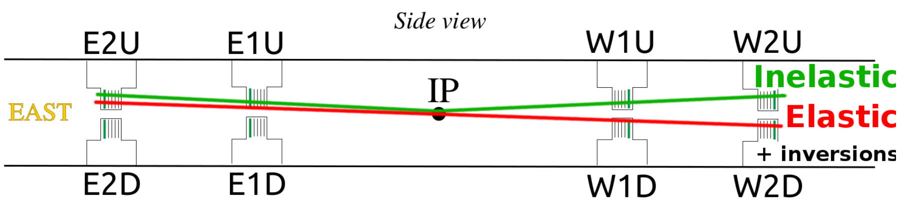

Fig. 4.1: The side view of the Roman Pot Phase II* setup with an illustration of Roman Pot track (in)elastic combinations. Taken from Ref. [4] and edited.

The following list describes each cut which is shown in the left Fig. 4.3 showing number of remaining events after application of each event cut. The exact number of events remaining after each cuts is shown in Tab. 4.2.

1. **All** - no cut or condition is applied at these stage.
2. **CPT trigger** - at least one of central production trigger, discussed above, was applied.
3. **El+InEl** - requirement of exactly 2 good quality tracks in Roman Pots and only elastic or inelastic combinations are accepted. The elastic and inelastic combinations are illustrated in Fig. 4.1. The track is reconstructed from two

track points. Each track point is reconstructed from up to four silicon planes. Only tracks with all 8 silicon planes used in their reconstruction are marked as good quality track. The illustration of track reconstruction is shown in Fig. 4.2.

4. **2 TPC-TOF tracks** - need for 2 TPC tracks matched with TOF as we are looking for $\pi^+\pi^-$ pair.

5. **Same vertex** - the tracks should be coming from the same vertex as they are produce by CEP.

6. **TotCharge 0** - the total charge of $\pi^+\pi^-$ pair should be zero.

7. $\mathbf{p_T^{miss} < 0.1}$ **GeV/c** - is the requirement of exclusivity. For this reason, we defined missing transverse momentum as follows

$$p_{\mathsf{T}}^{miss} = (\vec{p_1} + \vec{p_2} + \vec{\pi}_+ + \vec{\pi}_-)_{\mathsf{T}}, \tag{4.1}$$

where $\vec{p_1}, \vec{p_2}$ are momenta of outgoing protons and $\vec{\pi}_+, \vec{\pi}_-$ are momenta of produced $\pi^+\pi^-$. From the conservation of momentum the p_{T}^{miss} should be equal to zero. Since there is a track resolution of detector, we required $p_{\mathsf{T}}^{miss} < 100$ MeV, which is less than the mass of pion, the lightest meson. All pairs satisfying this cut are called exclusive pairs.

8. **PID** - particle identification is the last cut and it is discussed in next section.

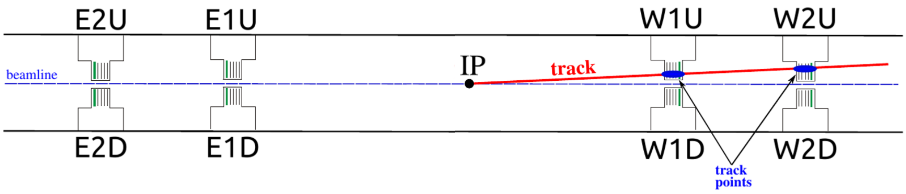

Fig. 4.2: The illustration of Roman Pot track reconstruction. Taken from Ref. [4] and edited.

Number of events remaining after the application of each event cut can be seen in Fig. 4.3. At the beginning, there were $24,261,132$ events at the trigger level. After application the event cuts, there are $1,477$ exclusive events with $\pi^+\pi^-$ pair remaining. The distribution of missing p_{T} of $\pi^+\pi^-$ pair event after three different event cuts is shown in Fig. 4.3. The peak from exclusive event is clearly visible.

4.2 Particle identification

At RHIC specific energies DIPE with $\pi^+\pi^-$ is expected to be dominant. The energy loss of charged particles measured in the TPC as a function of their transverse momentum and charge is shown in Fig. 4.5. Based on this measurement, most of the particles are pions, especially after the p_{T}^{miss} cut. For this reason, we defined $n\sigma_\pi^{pair}$ as follows

$$n\sigma_\pi^{pair} = \sqrt{\left(n\sigma_{\pi^+}^{trk}\right)^2 + \left(n\sigma_{\pi^-}^{trk}\right)^2}, \tag{4.2}$$

Cut	Number of remaining events
All	93, 845, 137
CPT trigger	24, 261, 132
El + InEl	3, 600, 390
2 TPC-TOF tracks	32, 500
Same vertex	31, 307
TotCharge 0	19, 641
$p_{\mathrm{T}}^{miss} < 0.1$ GeV/c	1, 554
PID	1, 477

Tab. 4.2: Number of events remaining after the application of event cuts.

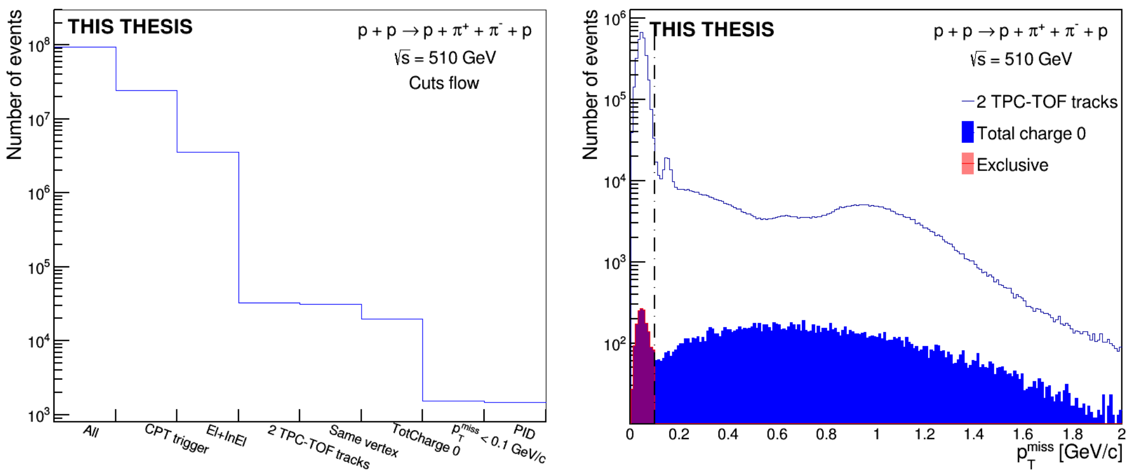

Fig. 4.3: Left: number of events remaining after the application of event cuts. Right: the distribution of missing p_{T} of pion candidates. The dotdash line indicates $p_{\mathrm{T}}^{miss} <$ 100 MeV cut.

where $n\sigma_{\pi^+}^{trk}$, $n\sigma_{\pi^-}^{trk}$ are variable obtained from TPC, which were introduced in Section 3.2.1. All pairs satisfying $n\sigma_{\pi}^{pair} < 3$ are assumed to be pions in this work. More complex PID is the subject of further work.

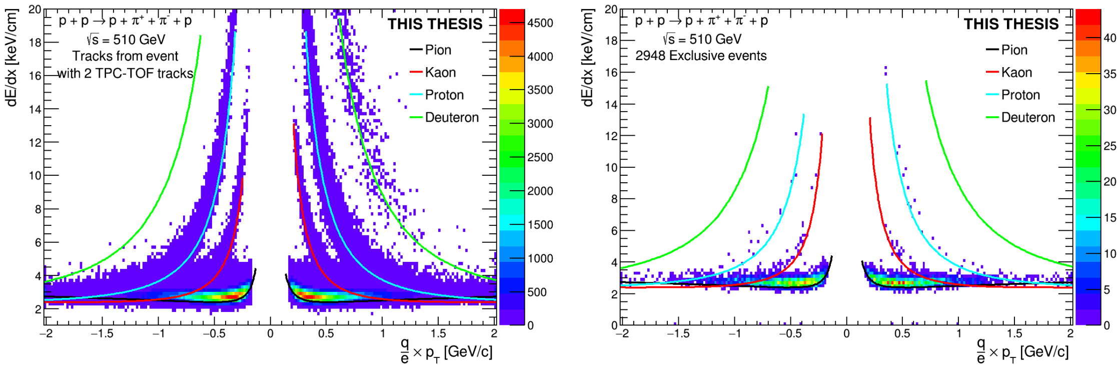

Fig. 4.4: The energy loss of charged particles as a function of their momentum and charge with Bichsel functions. Left: candidates with 2 TPC-TOF tracks. Right: candidates before PID cut is applied.

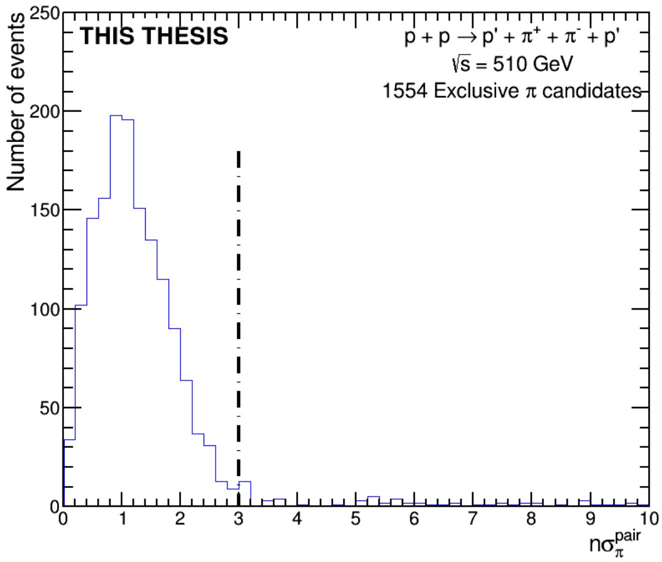

Fig. 4.5: The distribution of $n\sigma_{\pi}^{pair}$ of exclusive pairs. The dotdash line indicated the cut $n\sigma_{\pi}^{pair} < 3$.

4.3 Results

For all selected exclusive events with identified pion pair, the invariant mass of two TPC tracks was calculated by the following equation.

$$m_0 c^2 = \left(\frac{E}{c}\right)^2 - \vec{p}^2 \tag{4.3}$$

The first distribution of the invariant mass of $\pi^+\pi^-$ pairs at $\sqrt{s}$ = 510 GeV is shown in Fig. 4.6. The like-sign pion pairs are shown for comparison. The expected features can be seen: the broad structure extending from the production threshold to 1 GeV/c^2 followed with rapid drop and the significant resonant structure between $1.0 - 1.5$ GeV/c^2. This result is in good agreement with the previous measurement by the STAR experiment [14] (see Fig. 2.3) that validates the data set.

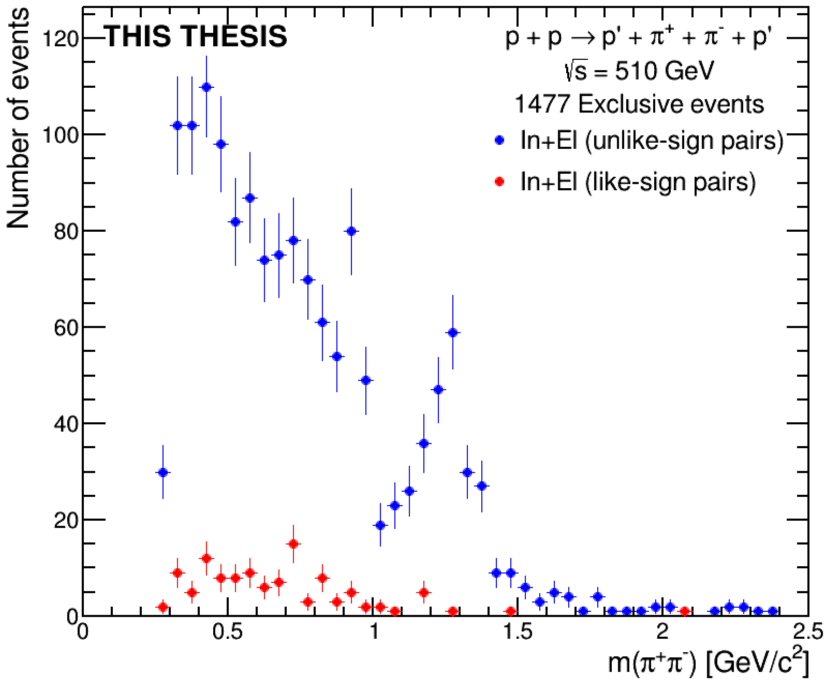

Fig. 4.6: The distribution of the invariant mass of $\pi^+\pi^-$ pairs. Distribution is not corrected for detector acceptance and efficiency. Error bars represent statistical uncertainty.

The picoDST production has been validated. The first distribution of the invariant mass of $\pi^+\pi^-$ pairs at $\sqrt{s} = 510$ GeV from the 5 % of run 17 can be seen in Fig. 4.7. For this result was used the same approach as discussed above. The expected resonant structure between $1.0 - 1.5$ GeV/c^2 is clearly visible together with the broad structure extending from the production threshold to 1 GeV/c^2. The broad structure shows different features than the on in Fig. 4.6 since the results were not corrected for acceptance, efficiencies etc.

In Fig. 4.8 the distribution of pseudorapidity of exclusive π candidates and the z-coordinate of reconstructed vertex of exclusive events is shown. Both variables are symmetrical around zero and show expected features. The data from run 17 were validated and they look promising.

The next step is to produce picoDST files for whole run 17 with about one billions events. We are expecting increase in statistic by factor of 4 compare to the previous measurement discussed earlier [14]. Furthermore, I am going to apply TPC/TOF track quality cuts, optimize the cuts and apply more complex PID methods, which allow to study processes with K^+K^- and $p\bar{p}$. In addition, the processes with $\pi^+\pi^-\pi^+\pi^-$ centrally produced state can be also analyzed.

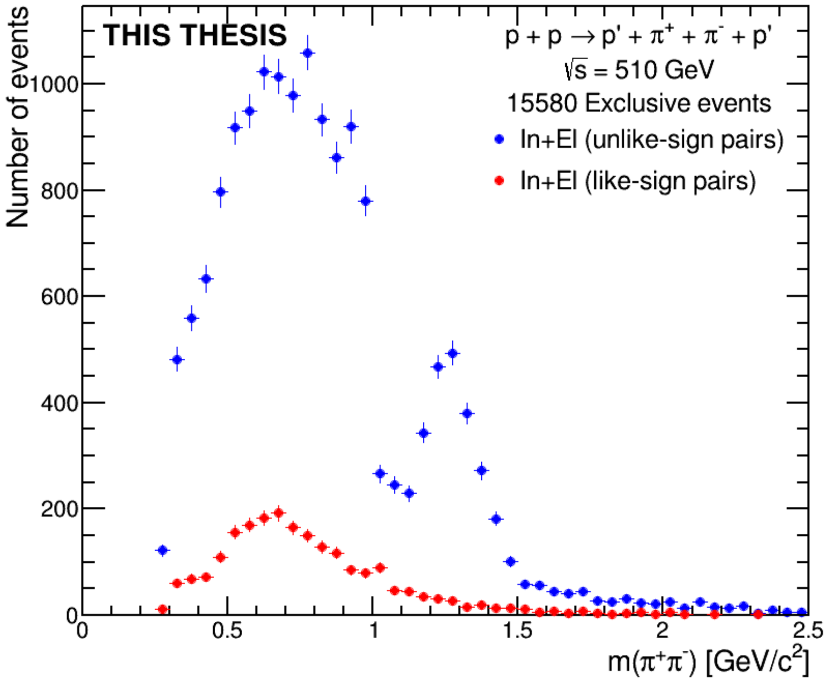

Fig. 4.7: The distribution of the invariant mass of $\pi^+\pi^-$ pairs. Distribution is not corrected for detector acceptance and efficiency. Error bars represent statistical uncertainty.

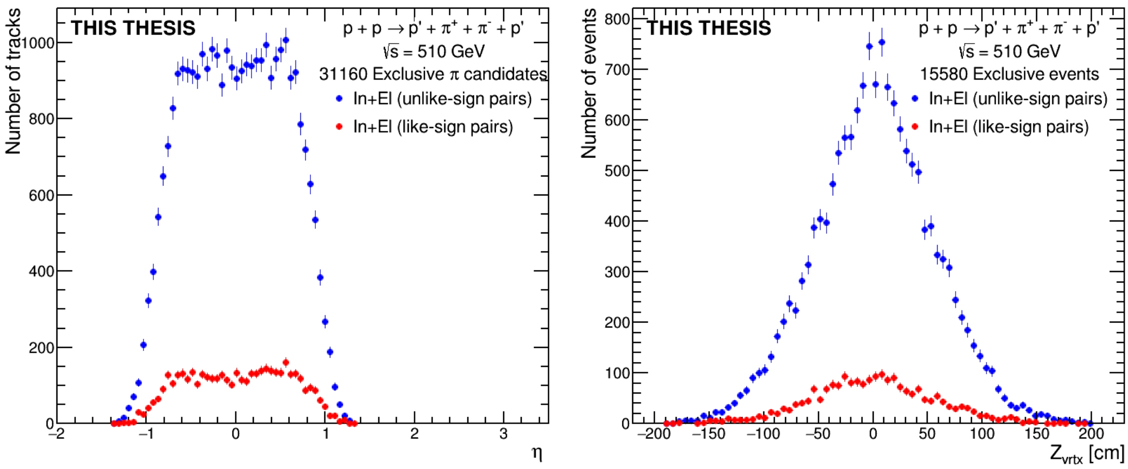

Fig. 4.8: Left: the distribution of pseudorapidity η of exclusive π candidates. Right: the distribution of Z_{vrtx}, the z-coordinate of reconstructed vertex, of exclusive events.

Summary

The goal of this work is to validate the picoDST production and data from proton-proton collisions at $\sqrt{s} = 510$ GeV which were recorded by the STAR experiment in 2017. Since this data set contains information from D$\mathbb{P}$E in CEP, it is promising for glueball search. The experimental confirmation of the existence of the glueball would be yet another strong support for the validity of the QCD theory. Therefore, it is important to analyze these data.

The first chapter of this work was an introduction to the high-energy diffractive physics. First, the kinematic variables were introduced, then, the hadronic diffraction physics was discussed. Furthermore, the Regge theory was presented included the introduction of $\mathbb{P}$omeron and glueball. The CEP as the potential source of glueballs was also introduced.

The second chapter provides the summary of recent results in central exclusive production, achieved by the experiments at CERN and by the STAR experiment. The features in the distribution of invariant mass of $\pi^+\pi^-$ and K^+K^- pairs have been discussed. The recent results indicate significant role of resonance production, however the exact nature of the features remains elusive.

The third chapter presented RHIC, the only major accelerator capable of colliding polarized protons, and the STAR experiment with its sub-detectors. STAR has unique capabilities such as: high-resolution tracking of charged particles in TPC, precise PID through the measurement of $\mathrm{d}E/\mathrm{d}x$ and Time-of-Flight, BBC covering forward rapidity $2.1 < |\eta| < 5.0$ to ensure rapidity gap and Roman Pots allowing measurement of forward protons. These features made STAR suitable detector for studying CEP processes.

Finally, the fourth chapter is dedicated to the first measurement of CEP in proton-proton collisions at $\sqrt{s} = 510$ GeV measured by the STAR experiment. Specifically, the distribution of invariant mass of $\pi^+\pi^-$ pairs has been presented. The distribution shows expected features and it is consistent with the previous measurement by the STAR experiment.

The data set and the picoDST production have been validated and the data look promising. The next step is to produce picoDST files for whole run 17 and apply more complex PID methods that allow to study processes with K^+K^- and $p\bar{p}$. Furthermore, I would like to also analyze the processes with $\pi^+\pi^-\pi^+\pi^-$ centrally produced state.

Bibliography

[1] S. M. Bilenky, *Introduction to Feynman diagrams*, [1st ed.] ed. New York: Pergamon Press, [1974].

[2] V. Barone and E. Predazzi, *High-energy particle diffraction.* New York: Springer, 2002.

[3] M. Pimenta and A. De Angelis, *Introduction to particle and astroparticle physics.* New York, NY: Springer Berlin Heidelberg, 2018.

[4] W. Guryn, et al, "Central Exclusive Production in Proton-Proton Collisions with the STAR Experiment at RHIC," *EPJ Web of Conferences*, vol. 120, no. 1, p. 5, 2016. [Online]. Available: http://www.epj-conferences.org/10.1051/epjconf/201612002008

[5] S. Donnachie, *Pomeron physics and QCD.* New York: Cambridge University Press, 2002.

[6] M.G. Albrow, et al, "Central exclusive particle production at high energy hadron colliders," *Progress in Particle and Nuclear Physics*, vol. 65, no. 2, pp. 149–184, 2010. [Online]. Available: https://linkinghub.elsevier.com/retrieve/pii/S0146641010000487

[7] CERN, "The Intersecting Storage Rings," https://home.cern/science/accelerators/intersecting-storage-rings, 2019, [Online; accessed 2019-08-01].

[8] D. Robson, "A basic guide for the glueball spotter," *Nuclear Physics B*, vol. 130, no. 2, pp. 328–348, 1977. [Online]. Available: https://linkinghub.elsevier.com/retrieve/pii/0550321377901109

[9] M. Albrow, "Double Pomeron Exchange: from the ISR to the LHC," *AIP Conference Proceedings*, vol. 1350, no. 1, pp. 119–123, 2011/07/15. [Online]. Available: https://aip.scitation.org/doi/abs/10.1063/1.3601389

[10] D. Denegri, et al, "Double pomeron exchange and diffractive dissociation in the reaction $pp \to pp\pi^+\pi^-$ at 69 GeV/c," *Nuclear Physics B*, vol. 98, no. 2, pp. 189–203, 1975. [Online]. Available: http://www.sciencedirect.com/science/article/pii/0550321375904289

[11] L. Baksay, et al, "Evidence for double Pomeron exchange at the CERN ISR," *Physics Letters B*, vol. 61, no. 1, pp. 89–92, 1976. [Online]. Available: https://linkinghub.elsevier.com/retrieve/pii/0370269376905700

[12] T. Åkesson, et al, “A search for glueballs and a study of double pomeron exchange at the CERN intersecting storage rings,” *Nuclear Physics B*, vol. 1986, no. 264, pp. 154–184, 1986. [Online]. Available: https://linkinghub.elsevier.com/retrieve/pii/0550321386904773

[13] CMS Collaboration, “Measurement of total and differential cross sections of central exclusive $\pi^+\pi^-$ production in proton-proton collisions at 5.02 and 13 TeV,” 2019.

[14] R. Sikora, “Recent results on Central Exclusive Production with the STAR detector at RHIC,” *Acta Physica Polonica B Proceeding Supplement*, vol. 2018, no. 1, p. 6, 2018.

[15] M. Harrison, et al, “RHIC project overview,” *Nuclear Instruments and Methods in Physics Research Section A: Accelerators, Spectrometers, Detectors and Associated Equipment*, vol. 499, no. 2, pp. 235–244, 2003. [Online]. Available: http://www.sciencedirect.com/science/article/pii/S016890020201937X

[16] M. J. Tannenbaum, “Highlights from BNL and RHIC 2015,” *The Future of Our Physics Including New Frontiers*, vol. 2016, no. 1, pp. 393–412, 2017-04-28. [Online]. Available: http://www.worldscientific.com/doi/abs/10.1142/9789813208292_0016

[17] D. Tlustý, “A Study of Open Charm Production in p+p Collisions at STAR,” Czech Technical University in Prague, 2014.

[18] A. R. Kesich, “Upsilon Production and Suppression as Measured by STAR in p + p, d + Au, and Au + Au Collisions at $\sqrt{s_{\mathrm{NN}}} = 200$ GeV,” University of California, 2014.

[19] T. Sugiura, “Exploring the QCD phase diagram measured by cumulants of net-charge distributions in Au+Au collisions at the STAR experiment,” University of Tsukuba, 2019.

[20] L. Adamczyk, et al, *Physical Review D*, vol. 86, no. 3, 2012. [Online]. Available: https://link.aps.org/doi/10.1103/PhysRevD.86.032006

[21] M. Anderson, et al, “The STAR time projection chamber: a unique tool for studying high multiplicity events at RHIC,” *Nuclear Instruments and Methods in Physics Research Section A: Accelerators, Spectrometers, Detectors and Associated Equipment*, vol. 499, no. 2-3, p. 20, 2003.

[22] H. Bichsel, “A method to improve tracking and particle identification in TPCs and silicon detectors,” *Nuclear Instruments and Methods in Physics Research Section A: Accelerators, Spectrometers, Detectors and Associated Equipment*, vol. 562, no. 1, pp. 154–197, 2006. [Online]. Available: https://linkinghub.elsevier.com/retrieve/pii/S0168900206005353

[23] J. Fodorová, “Production of J/Ψ meson in central U+U collisions at the STAR experiment,” Czech Technical University in Prague, 2016.

[24] R. Líčeník, “Study of D meson production in 200 GeV Au+Au collisions at the STAR experiment,” Czech Technical University in Prague, 2019.

[25] J. Schambach, "Proposed STAR Time of Flight Readout Electronics and DAQ," *Computing in High Energy and Nuclear Physics, LaJolla, California*, vol. 2003, no. 1, p. 10, 2003.

[26] K. Kajimoto, "A large area time of flight detector for the STAR experiment at RHIC," The University of Texas at Austin, 2019.

[27] C. A. Whitten, et al, "The Beam-Beam Counter," *AIP Conference Proceedings*, vol. 2008, no. 1, pp. 390–396, 2008. [Online]. Available: http://aip.scitation.org/doi/abs/10.1063/1.2888113

[28] R. Sikora, "Central exclusive production in the STAR experiment at RHIC," *AIP Conference Proceedings*, vol. 2017, no. 1819, 040012, p. 4, 2017. [Online]. Available: http://aip.scitation.org/doi/abs/10.1063/1.4977142

[29] M. Oriunno, et al, "The Roman Pot forthe LHC," *Proceedings of EPAC*, vol. 2006, no. MOPLS013, p. 3, 2006.

[30] S. Bültmann, et al, "The PP2PP experiment at RHIC: silicon detectors installed in Roman Pots for forward proton detection close to the beam," *Nuclear Instruments and Methods in Physics Research Section A: Accelerators, Spectrometers, Detectors and Associated Equipment*, vol. 535, no. 1-2, p. 6, 2004.

[31] R. Sikora, "Study of elastic proton-proton scattering with the STAR detector at RHIC," AGH University of Science and Technology, 2014.